# GAP JUNCTION UNCOUPLING AND DISCONTINUOUS PROPAGATION IN THE HEART

## A Comparison of Experimental Data with Computer Simulations

WILLIAM C. COLE, JOHN B. PICONE, AND NICHOLAS SPERELAKIS
*Department of Physiology and Biophysics, University of Cincinnati College of Medicine, Cincinnati, OH 45267*

ABSTRACT The effects of octanol on longitudinal propagation in guinea pig papillary muscles were measured by intracellular microelectrodes. These data were compared with alterations in conduction induced by stepwise removal of gap junction channels in computer simulations of propagation based on a discontinuous cable model. Octanol reduced the velocity ($\theta$) of propagating action potentials (APs) from 53.2 ± 3.5 to <6.6 ± 2.1 cm/s before block occurred. The maximal rate of rise ($\dot{V}_{max}$) changed in a biphasic manner, increasing from 133.1 ± 5.4 in controls to 201.7 ± 11.0 V/s when $\theta$ was 20.5 ± 2.8 cm/s, and then declining to <58.6 ± 15.2 V/s just before block. The input resistance and time constant of the AP foot increased, and the ascending limb of phase-plane loops became increasingly nonlinear and notched during octanol treatment. All effects of octanol reversed upon washout. A strand of cardiac tissue was modeled as a discontinuous cable composed of 40 cells, each with 10 isopotential membrane segments described by Beeler-Reuter kinetics, and coupled by a variable number of gap junction channels (156 pS). Decreasing the number of channels from 40,000 to 400 to 60 slowed conduction from 62.6 to 16.4 to 3.1 cm/s. As noted in the experimental data, $\dot{V}_{max}$ increased from 103 to 130 and then fell to <96 V/s. The AP foot increased and became nonexponential. Distinct notches developed during phase 1 of the APs at slower propagation velocities in the experiments and simulations. The close similarities between the experimental and theoretical data obtained in this study supports the applicability of a discontinuous cable model for describing longitudinal propagation in the heart.

### INTRODUCTION

In general, the passive and active electrical properties of cardiac muscle have been mathematically analyzed (e.g., Weidmann, 1952; Woodbury and Crill, 1961; Weidmann, 1970; Bonke, 1973; Carmeliet and Willems, 1971; Clerc, 1976; DeMello, 1977) as though the tissue were a simple cablelike structure similar to that of an axon, i.e., classical continuous cable theory (Hodgkin and Rushton, 1946; Hodgkin and Huxley, 1952). This analysis assumes (*a*) that current spread in a bundle of myocardial cells is equivalent to that in a simple cable of uniform internal resistance and cross-sectional diameter, and (*b*) that the cable lies in a large volume conductor, such that there is parallel current flow in the intracellular and extracellular compartments at all distances from the source. The velocity of propagation ($\theta$) and shape of conducted action potentials (APs) are predicted to be constant and homogeneous, such as occurs in axons or skeletal muscle.

Address correspondence to Nicholas Sperelakis, Dept. of Physiology and Biophysics, ML 576, 231 Bethesda Ave., Cincinnati, OH 45267-0576.

William Cole's present address is Dept. of Physiology, University of Nevada, Reno, NV 89557.

However, continuous cable theory ignores the fact that the myocardium is a complex three-dimensional assembly of branching and converging bundles. Each bundle consists of elongated individual cells of nonuniform dimension and shape, which are joined by a variable number of gap junctions and separated from each other by a confined interstitial space of variable dimension (Forbes and Sperelakis, 1985). It is apparent that this complex structure influences propagation to produce phenomena that are inexplicable by continuous cable theory.

For example, it has been recognized for some time that phase-plane analysis of propagating APs in cardiac tissue yields loop contours that differ appreciably from those obtained for homogeneous conduction in nerve or skeletal muscle (Sperelakis and Shumaker, 1968; Paes de Carvalho et al., 1969; Paes de Carvalho, 1975; Paes de Carvalho et al., 1982). The rising phase of the upstroke loops recorded from cardiac cells are often distinctly nonlinear, implying that there are local changes in the velocity (i.e., microaccelerations or -hesitations) of activity propagating in a direction parallel or transverse to the long axis of the cells (Paes de Carvalho et al., 1982). Moreover, studies involving computer simulations imply that the discrete cellular structure of the cells and presence of gap junctions

influences action potential shape, maximal rate of rise ($\dot{V}_{max}$), and propagation velocity in a manner that is clearly at odds with that predicted by continuous cable theory (Joyner, 1982; Diaz et al., 1983; Henriquez and Plonsey, 1986; Myers and Maglaveras, 1986; Rudy and Quan, 1986).

In the present study, we compared computer simulations of propagation in cardiac tissue based on a discontinuous cable model with propagation along the longitudinal axis of small papillary muscles under conditions of elevated intercellular resistance. Increased intercellular resistance was modeled in the computer simulations by reducing the number of gap junction channels between adjoining cells. This was compared with alterations in propagation in papillary muscles after exposure to octanol. Long-chain alcohols, such as octanol and heptanol, have been shown to block propagation in cardiac muscle and other tissues (Johnston et al., 1980; Joyner and Overholt, 1985), to alter gap junction morphology (Bernardini et al., 1984; Déleze and Hervé, 1986), to depress electrotonic coupling in isolated cardiac cell pairs (White et al., 1985), and to block single channel activity of cardiac gap junctions (Veenstra and De Haan, 1986). The results of this study support the applicability of a discontinuous cable model to describe longitudinal propagation in cardiac tissue. Preliminary accounts of some of these data have appeared previously (Picone et al., 1987; Cole et al., 1987).

## METHODS

### Computer Simulation

We have taken the Heppner-Plonsey (Heppner and Plonsey, 1970) resistive arrangement for the intercalated disc and modified it to describe the gap junction cell-to-cell channels in a more explicit manner. $R_{gj}$ in Fig. 1 represents the longitudinal pathway for cell-to-cell current flow. It is the effective axial resistance of one or more junctional channels, each being 156 pS (Veenstra and DeHaan, 1986) with the value of the resistance determined according to Ohm's law for parallel resistances. $R_{wall}$ represents the resistance of the protein wall of the junctional channels and is assumed to have a resistance at least as large as that of the lipid bilayer of a cell membrane. It limits the amount of current lost to the extracellular space across the cleft shunt resistance, $R_{shunt}$. $R_{shunt}$ is estimated by the following formula, given by Katz (1966): $R_{shunt} = \rho_{isf}/(8\pi\,\delta)$, where $\rho_{isf}$ is the resitivity of the interstitial fluid, and $\delta$ is the cleft width. An extensive discussion on the cleft resistance can be found in Mann et al. (1977). The resistive network shown in Fig. 1 provides a convenient method for modeling changes in cell-to-cell coupling resulting from specific alterations in the number of junctional channels or their unit conductance.

To simulate propagation along a one-dimensional strand of cells connected by gap junctional channels we have combined the resistive network described by Heppner and Plonsey (1970) with a discrete cable model similar to that of Diaz et al. (1983). A thin cylindrical strand of cardiac tissue lying in a large volume conductor was modeled as shown in Fig. 1. This strand was considered to consist of 40 cells joined end-to-end by intercalated discs (Fig. 1, *top*). Each cell was broken up into 10 elements that represent discrete isopotential segments of membrane (Fig. 1, *middle*). Each cell was connected to the next by a variable number of gap junction channels (Fig. 1, *bottom*). The values used for the various parameters indicated in Fig. 1 are listed in Table I.

The membrane conductances of each membrane segment in Fig. 1 are given by the Beeler-Reuter (B-R) model for ventricular membrane

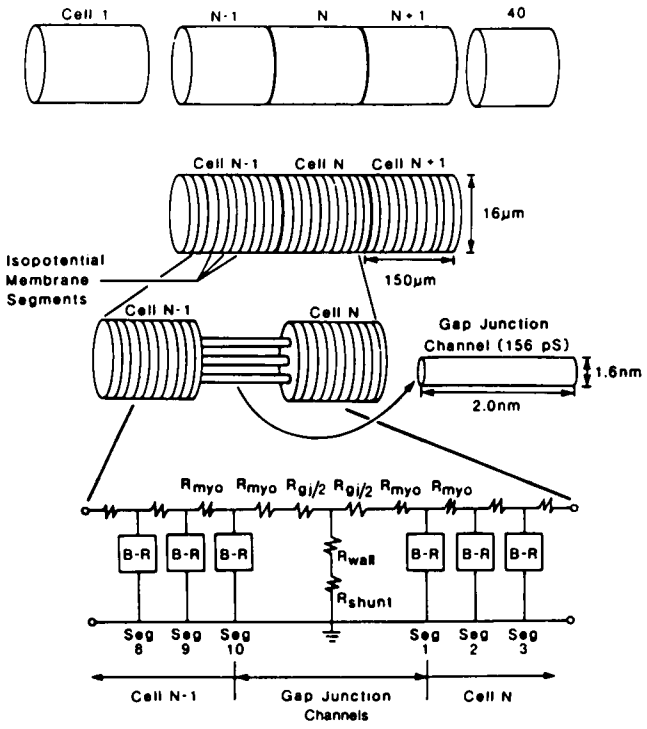


FIGURE 1 Theoretical model of a strand of cardiac tissue. A model for a thin cylindrical strand of cardiac tissue composed of 40 cells joined end-to-end and lying in a large volume conductor. The cells are 150 μm in length, 16 μm in diameter, and discretized into 10 segments. Each segment represents an isopotential patch of membrane capable of generating action potentials according to the Beeler-Reuter description for ionic currents in ventricular myocardial cells. Lying between each pair of cells are a variable number of gap junction channels, each 2.0 nm in length and 1.6 nm in diameter, with a conductance of 156 pS. The lower part of the figure illustrates a portion of the equivalent electrical circuit used for modeling the strand of cardiac cells. The isopotential membrane segments are represented by Beeler-Reuter (B-R) units and are linked together by resistances calculated from $R_{myo}$, the myoplasmic resisitivity. The gap junction region is shown as a T-network of resistances. $R_{gj}$ is the longitudinal current pathway of one or more gap junction channels; $R_{wall}$ is the resistance across the channel wall; and $R_{shunt}$ is the resistance between the junctional cleft and the extracellular space.

currents (Beeler and Reuter, 1977). Within the cell, the membrane segments are separated from one another by a longitudinal resistance based on a specific intracellular resistivity ($R_{myo}$) of 200 Ω-cm. The actual resistive value in ohms is calculated from $R_{myo} \cdot \Delta x$, where $\Delta x$ represents the distance from the center of one isopotential segment to the center of the next. We numerically solved for the membrane voltage as a function of longitudinal position and time using the Crank-Nicholson method for implicit integration of parabolic differential equations (Crank and Nicholson, 1947). This method has been applied previously in modeling propagation in axons and cardiac fibers (Joyner et al., 1978; Sharp and Joyner, 1980), and involves the simultaneous solution of a system of equations, one for each node. In brief, Kirchoff's law for conservation of current is applied to each node and the resulting voltage distribution in space and time is expressed as a difference equation using the time average for the second central difference form of the spatial derivative. Within any given cell, as in a uniform cable, this is equivalent to writing the cable equation

$$\partial^2 V/\partial x^2 = R_i[C_m(\partial\, V/\partial\, t) + I_{ion}] \qquad (1)$$

TABLE I
VALUES OF SIMULATION PARAMETERS

| | |
|---|---|
| No. of cells | 40 |
| Cell length | 150 $\mu$m |
| Cell radius | 8 $\mu$m |
| No. of membrane patches per cell | 10 |
| Gap junction channel length | 2.0 nm |
| Gap junction channel radius | 0.8 nm |
| Gap junction channel conductance ($R_{gj}$) | 156 pS |
| Gap junction channel membrane resistance ($R_{wall}$) | 1,000 $\Omega$-cm$^2$ |
| Specific membrane resistance ($R_m$) | 1,000 $\Omega$-cm$^2$ |
| Specific membrane capacitance | 1 $\mu$F/cm$^2$ |
| Specific intracellular resistivity ($R_{myo}$) | 200 $\Omega$-cm |
| Cleft shunt resistance ($R_{shunt}$) | 2 M$\Omega$ |

in its difference form. The result is a set of equations, one for each node, with the following form:

$$B_j \cdot V_{j-1}^{t+\Delta t} + D_j \cdot V_j^{t+\Delta t} + A_j \cdot V_{j+1}^{t+\Delta t} = C_j$$

$$j = 1, 2, 3, \ldots \text{No. nodes}$$

$$B_j = Z$$

$$D_j = -2(Z + 1)$$

$$A_j = Z$$

$$C_j = -Z \cdot V_{j-1}^t + (2Z - 2) \cdot V_j^t - Z \cdot V_{j+1}^t \cdot (2 \cdot \Delta t / C_m) I_{ion}, \quad (2)$$

where $Z = \Delta t / R_i C_m \Delta x^2$.

The term $I_{ion}$ represents the total ionic current per unit length, and is computed from the Beeler-Reuter model. For those nodes within or immediately adjacent to the gap junctions, the difference equations share the same form as the above expression but possess different coefficients. These differences arise as a result of using the $R_{wall}$, $R_{shunt}$, and $R_{gj}$ resistances in place of the B-R elements. The final combination of all nodal voltage expressions generates a system of $X$ differential equations in $X$ unknowns that must be solved for simultaneously at each time step. Using the voltages at time $t$, the solution algorithm computes $I_{ion}$ for each membrane patch in the strand and then solves for voltages at the next time step, $t + dt$. The initial conditions used to compute the standard action potential with the B-R model are as follows: $m = 0.01126$, $h = 0.9871$, $j = 0.9927$, $x_1 = 0.0241$, $d = 0.0030$, $f = 1.0$, $[Ca]_i = 1.792E\text{-}07$, and $V_m = -84.35$ (Sharp and Joyner, 1980). For some simulations, the sodium inactivation process was slowed by simply multiplying the time constants of the inactivation variables, $\tau_h$ and $\tau_j$, by a factor of 100. Because of its implicit nature, the Crank-Nicholson method converges and produces stable solutions of membrane potential as a function of distance and time. The simulations were run on a VAX 11/750 computer system.

## Experiment

Guinea pigs (200–250 g) were anesthetized with $CO_2$ and killed by cervical dislocation. Their hearts were quickly removed and placed in a dish containing cold Tyrode solution with a composition in mM: NaCl, 114.3; KCl, 4.7; $MgCl_2$, 0.8; $CaCl_2$, 2.0; $NaHPO_4$, 1.7; $NaHCO_3$, 25; glucose, 11, and a pH of 7.4 when gassed with 95% $O_2$/5% $CO_2$. Thin papillary muscles with a cross-sectional diameter of 0.5 mm or less were quickly dissected from the right ventricle and pinned to the floor of a Sylgard (Dow Corning Corp., Midland, MI)–coated perfusion chamber. The chamber was superfused with a well-oxygenated Tyrode solution at 37°C at a rate of 1 ml/min and the muscle stimulated by square pulses delivered by a point source at a rate of 0.5 Hz and duration of 2 ms for an equilibration period of at least 30 min before recording transmembrane potentials. After obtaining control measurements, the tissues were exposed to Tyrode solution containing octanol (Sigma Chemical Co., St. Louis, Mo; 0.048–0.48 $\mu$ l/ml). Unless indicated otherwise, data are for experiments using 0.48 $\mu$ m/ml. Exactly similar observations were made at lower concentrations of octanol but it took considerably longer (45–60 min) for the initiation of any changes in propagation. The octanol solutions were prepared by vigorous shaking on a Vortex Genie just before use. After the measurements of propagation were made using octanol-containing solutions, the tissues were reexposed to normal Tyrode solution to demonstrate reversibility of the drug effects.

Transmembrane potentials were recorded with one or two conventional microelectrodes filled with 3 mM KCl connected to Dagan 8500 microelectrode preamplifiers. The maximum rate of rise ($\dot{V}_{max}$) of the action potentials (APs) was obtained by recording the first derivative ($dV/dt$) of the APs with a passive differentiator. Records of $V$ and $dV/dt$ as a function of time and in the phase-plane ($V$ on the abscissa and $dV/dt$ on the ordinate) were displayed on a Textronix 5111 storage oscilloscope and recorded to floppy disc using an IBM XT computer and Computerscope ISC-16 data acquisition system.

Propagation velocity was determined from the time required for APs to propagate between impaled cells at a known distance of separation. To ensure that only longitudinal propagation was measured, the microelectrodes were carefully positioned along the same axis of the papillary muscles as the stimulating electrode. Whenever possible, three different values for the propagation velocity were calculated based on the distance between the site of stimulation and the two recording electrodes, respectively, and on the intrarecording electrode distance. If $\theta$ values calculated for these three distances differed by >2.0% then new sites for measurement were chosen. In some instances (as in Fig. 6), one of the pair of the pipettes was placed adjacent to the site of stimulus to observe membrane action potential. In these cases, $\theta$ was calculated from the time delay between the stimulator artifact and the time to reach the $\dot{V}_{max}$ peak during the depolarizing phase of the AP at the second site of impalement. The time constant of the foot of the APs ($\tau_{foot}$) was determined from the initial slope of the first 10 mV of depolarization from resting potential on a semilog plot. The input resistance ($R_{in}$) of impaled cells was determined using a Wheatstone bridge circuit. The bridge circuits were always balanced before cell penetration to a null point where there were no DC voltage shifts in response to small hyperpolarizing current pulses (2–20 nA) and checked for balance upon withdrawal from the cell. $R_{in}$ was calculated from the slope of I-V plots for current pulses of varying magnitude.

# RESULTS

## Computer Simulations

The results of our computer simulations are similar to those of Diaz et al. (1983) and Rudy and Quan (1986). Fig. 2 shows plots of propagating APs along a strand consisting of 40 cardiac cells, where each cell was joined to the next by the indicated number of gap junction channels. We differentiate between propagation along the cell membrane and across the junctional cleft by plotting the voltage changes for each of the 10 successive membrane segments of the two cells at the center of the strand, i.e., cell Nos. 19 and 20. The left-most curves in each panel of Fig. 2 show the firing of the 10 membrane units in cell 19. The right-most curves show the activity in cell 20. It is clear from this figure that even when the cells are well coupled by junctional channels (i.e., 40,000), there is a finite time delay as the AP propagates across the junctional cleft from the last membrane segment in cell No. 19 to the first in No. 20. This delay at the cleft became more evident as the number of junctional channels was reduced as is shown in

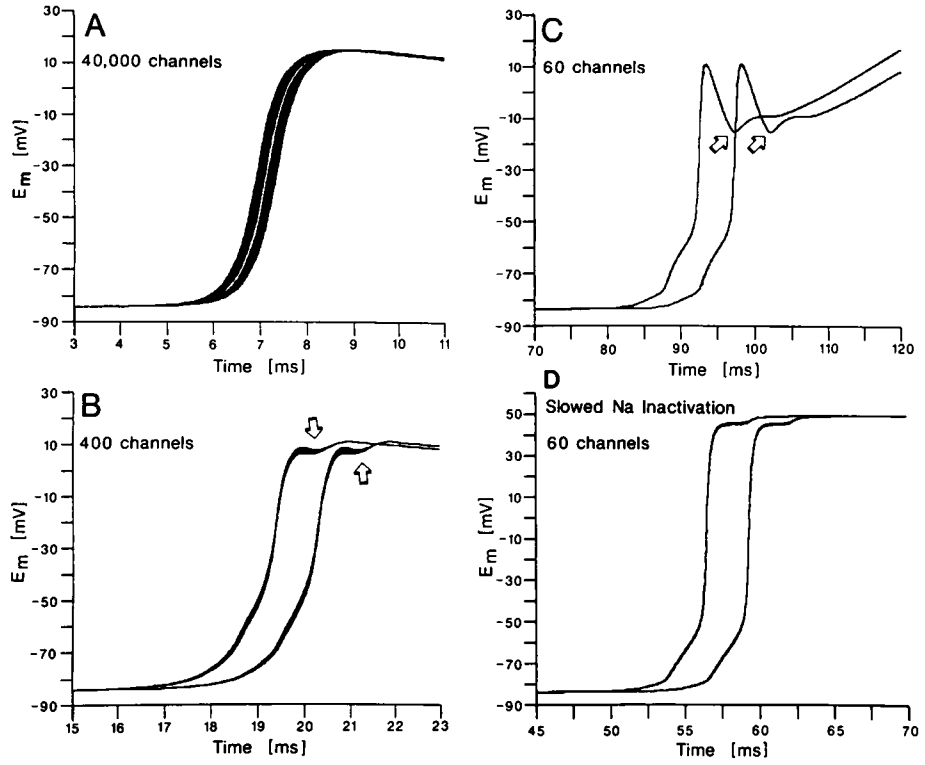


FIGURE 2 Effect of cell-to-cell uncoupling on a propagating action potential (computer simulations). Action potential propagation from cell Nos. 19 to cell 20 in a strand of cardiac tissue 40 cells in length (see Fig. 1) as the number of gap junction channels is varied. Action potentials are shown propagating through the 10 membrane segments of cell No. 19, across the cleft region, and through the 10 membrane segments of cell No. 20. Note the different time scales in the different panels. (*A*) 40,000 channels between each pair of cells. There is a small conduction delay of 0.065 ms at the cleft. (*B*) 400 channels between each pair of cells. The width of the vertical bands generated by the membrane segments of cell Nos. 19 and 20 is less than in *A*, indicating faster activation of the B-R units within each cell. There is also an increased conduction delay of 0.890 ms at the cleft. Note the development of a notch (see arrows) during phase 1 repolarization. (*C*) 60 channels between each pair of cells. The conduction delay at the cleft is greater (4.80 ms) and the phase 1 notch has increased significantly. Furthermore, the extreme thinness of the vertical bands indicates virtually instantaneous activation of the B-R membrane units in each cell. (*D*) 60 channels between each pair but the Na inactivation kinetics were slowed by increasing $\tau_h$ and $\tau_j$ by a factor of 100. Comparing to Fig. 2 *C*, note the increased conduction velocity (conduction delay at the cleft is 2.84 ms), the increased action potential amplitude, and the obvious decrease in the phase 1 notch.

Fig. 2, *B* and *C*, where only 400 or 60 channels were present between each cell within the strand. (Note the different time scales in the different panels.) As the number of channels was reduced, the conduction velocity ($\theta$) declined. This is evident in Fig. 2, *B* and *C*, from the greater time required for the AP to reach cell No. 20. Note also that the time required for all membrane units within a given cell to fire (reflected by the width of the trace) decreases as the number of channels is reduced. Arrows in Fig. 2, *B* and *C*, indicate the presence of a distinct phase 1 notch. These notches appeared after $\dot{V}_{max}$ had attained its peak value, and increased in size until propagation block.

The relationship between the extent of coupling, propagation velocity ($\theta$), and $\dot{V}_{max}$ is illustrated in Fig. 3, where $\theta$ (3 *B*), and $\dot{V}_{max}$ (3 *A*) are plotted as a function of the number of junctional channels between the cells. The velocity was calculated using the time delay for the AP to propagate between cells 10 and 30. It is shown to decrease with fewer numbers of junctional channels, declining from a plateau of ~63 cm/s at 40,000 channels, above which any

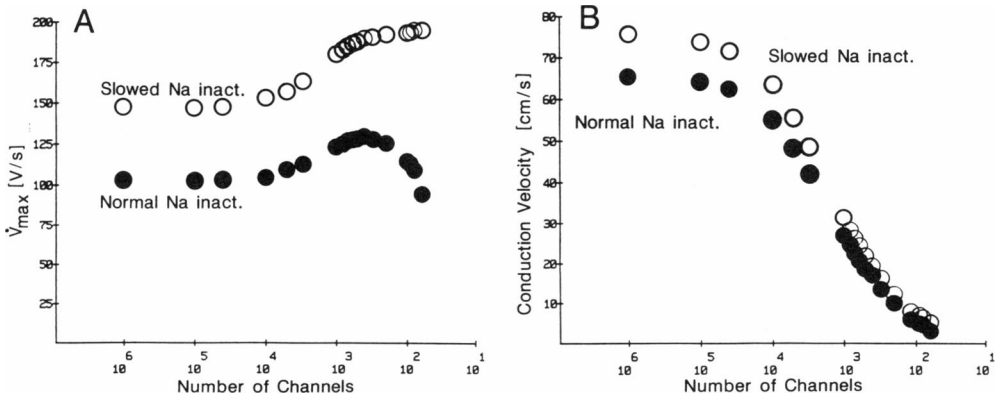


FIGURE 3 Effect of cell-to-cell uncoupling on $\dot{V}_{max}$ and conduction velocity (computer simulations). Maximal upstroke velocity ($\dot{V}_{max}$) (*A*) and overall conduction velocity (*B*) are plotted as functions of the number of gap junction channels between cells. Values are from the strand described in Fig. 1. $\dot{V}_{max}$ is measured across the middle segment of cell No. 20; conduction velocity is measured between cell Nos. 10 and 30. Solid curves show the effects of uncoupling given normal Na inactivation kinetics. As the number of channels is reduced, $\dot{V}_{max}$ increases from a value of 103 V/s at 40,000 channels, to a maximum of 130 V/s at 400 channels, and then drops as the cells become completely uncoupled at ~60 channels. Conduction velocity gradually falls from a value of 62.6 cm/s at 40,000 channels to a value of 3.12 cm/s at 60 channels. Dashed curves show the effects of uncoupling in the same strand except that the time constants of the Na inactivation variables *h* and *j* ($\tau_h$, $\tau_j$) have been increased by a factor of 100. Increasing $\tau_h$ and $\tau_j$ slows the Na inactivation process and prevents the sudden drop in $\dot{V}_{max}$ otherwise observed when the number of channels falls below 400.

further increase in the extent of cell-to-cell coupling has little effect on propagation velocity (Fig. 3 *B*). Below 60 channels the velocity falls under 3 cm/s as the cells become effectively uncoupled and conduction is blocked.

Fig. 3 *A* shows that as the number of junctional channels is decreased, $\dot{V}_{max}$ changed in a biphasic manner; initially it increased to a maximal value of 130 V/s when there were 400 channels and a velocity of 16.4 cm/s. It subsequently decreased until propagation was blocked. This biphasic change in $\dot{V}_{max}$ departs from the monotonic behavior predicted by continuous cable theory. $\dot{V}_{max}$ is often used as an indirect measure of the membrane ionic currents, and in a uniform continuous cable it is not expected to change if the membrane properties do not change. Fig. 3 also illustrates the effects on $\theta$ and $\dot{V}_{max}$ of increasing the time constants of the sodium channel inactivation variables, $\tau_h$ and $\tau_j$, in the Beeler-Reuter units by a factor of 100. For this case, $\theta$ was initially higher, as expected, and $\dot{V}_{max}$ increased to a maximum as coupling and propagation velocity decreased. Note, however, that the falling phase on the $\dot{V}_{max}$ curve was eliminated and the rate of rise remained high until the cells were completely uncoupled and propagation was blocked. Altering Na inactivation in this manner also eliminated the development of the phase 1 notch under conditions of reduced coupling. This may be seen by comparing the APs in Fig. 2 *D*, in which Na inactivation was slowed, with those in Fig. 2 *C*.

The foot of propagating APs increased in the simulations when the number of channels was decreased (Fig. 4). Additionally, note the distinct departure from an exponential rise in voltage during the foot as the number of channels is reduced. This nonexponential behavior is also evident in the phase-plane plots of Fig. 5. The initial

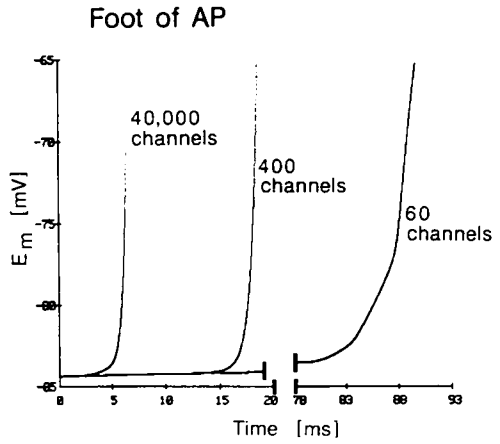


FIGURE 4 Effect of cell-to-cell uncoupling on the foot of the action potential (computer simulations). Plots of the foot of a propagating action potential from the middle membrane segment of cell No. 20 in a 40-cell strand (see Fig. 1). Voltage is plotted for the first 20 mV of depolarization from rest, i.e., −84.35 mV to −65 mV. Three cases are shown: (*A*) 40,000 channels between cells; (*B*) 400 channels between cells; and (*C*) 60 channels between cells. Note the amount of time required for depolarization increases as the number of gap junction channels is reduced.

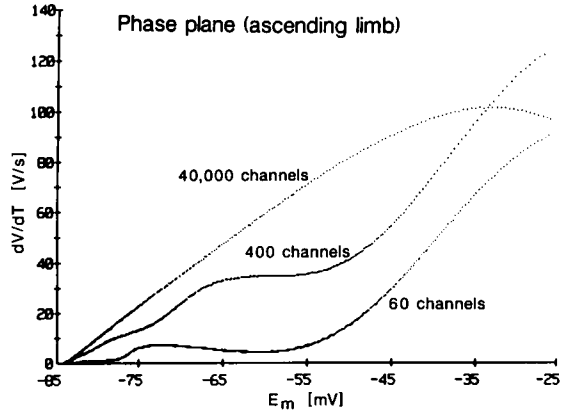


FIGURE 5 Effect of cell-to-cell uncoupling on the phase-plane of the propagating action potential (computer simulations). Phase-plane plots of a propagating action potential from the middle membrane segment of cell No. 20 in a 40-cell strand (see Fig. 1). The upstroke velocity ($dV/dt$) is plotted as a function of voltage (mV) over the range −84 mV (resting potential) to −25 mV. Three cases are shown: (*A*) 40,000 channels between cells; (*B*) 400 channels between cells; and (*C*) 60 channels between cells. Note the increasing degree of nonlinearity of the initial slope as the number of gap junction channels is reduced.

portion of the loops is shown to become increasingly nonlinear as the cells are uncoupled.

In the simulations above, the cell length of each myocyte in the chain was considered to be 150 μm, which is at the upper limit of ventricular fibers. For this reason we also ran simulations using a chain consisting of 40 cells, each being 75 μm in length. The results were qualitatively identical and differed only slightly in quantitative terms from those using 150-μm cells.

## Experiment

Fig. 6 shows that octanol (0.48 μl/ml) treatment reversibly blocks AP propagation in guinea pig papillary muscles. The series of intracellular recordings illustrates the sequential changes in APs propagating between two sites on a papillary muscle during exposure to octanol. In this experiment, microelectrode No. 1 was situated immediately adjacent to the site of stimulation, and was separated from No. 2 by 0.74 mm. The increase in the delay between the firing of cell Nos. 1 and 2 in sequential recordings reflects a drop in the propagation velocity from 63.4 cm/s to <4.5 cm/s just before block. Relatively little change in the delay to firing of cell No. 1 was noted with the electrodes in this arrangement. Note the presence of a distinct notch creating a prominent phase 1 on the APs recorded from cell No. 2 in Fig. 6, *C–E*. With the electrodes in this arrangement, the notch was always restricted to cell No. 2. Also note that when the impaled cell was next to the stimulus site it was still capable of firing a membrane AP after propagation block had occurred. Stray capacitive transients were also occassionally noted on the traces.

In Fig. 7 *A* both microelectrodes were placed at some distance from the stimulation site and were only separated

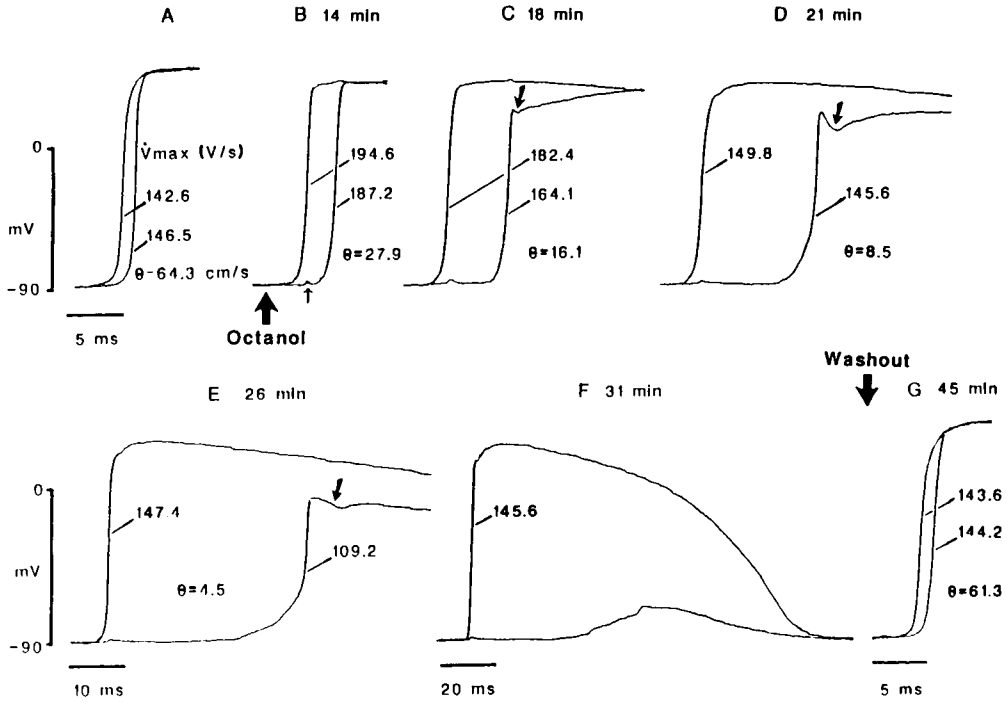


FIGURE 6 Effect of octanol on propagating action potentials in guinea pig papillary muscles. This series of intracellular recordings (*A–E*) show the results of an experiment in which octanol (0.48 μl/ml) was used to influence propagation along the longitudinal axis of a small papillary muscle (0.5 × 4.0 mm). In this case one microelectrode was placed adjacent to the site of stimulation and separated from the second electrode by 0.74 mm. $\theta$ at site No. 2 was determined from the latency between the stimulus artifact and the voltage at which $\dot{V}_{max}$ was achieved. Values of $\dot{V}_{max}$ (V/s) and $r$ (cm/s) are given in each panel. Octanol is shown to cause (*a*) a progressive decrease in $\theta$ (*A–E*) and eventual propagation block (*F*), (*b*) a biphasic change in $\dot{V}_{max}$ (cell 2 in *A–E*), and (*c*) alterations in AP shape, as evidenced by the development of a notch during phase 1 of the propagating APs recorded from cell No. 2 in *C–E* (*large arrows*). Note also the capacitive transients (*small arrow*) *in B*. *G* indicates that the effects of octanol were completely reversible.

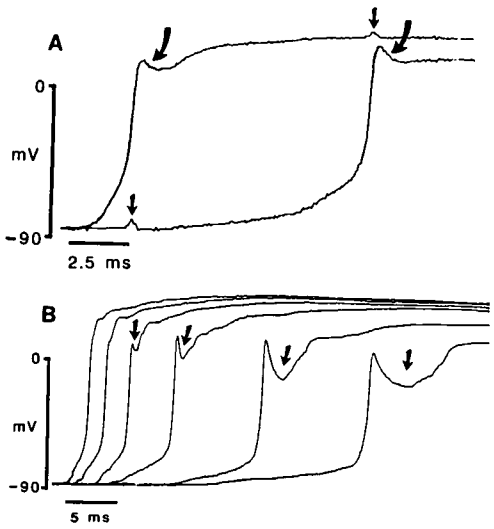


FIGURE 7 Phase 1 notch development during octanol treatment. (*A*) Phase 1 notches (*large arrows*) were observed in recordings from both cells when the microelectrodes were placed at some distance from the stimulation site. In this case the microelectrodes were separated by 0.19 mm and $\theta$ was 1.9 cm/s after 28 min of octanol treatment (0.48 μl/ml). ($\theta$ determined from the latency between voltages at which $\dot{V}_{max}$ was achieved in the two cells.) Capacitive transients (*small arrows*) are apparent on recordings from both cells. (*B*) This sequence of recordings from a single cell documents the development of the phase 1 notch (*arrows*) during octanol treatment. The first trace was recorded at 15 min and the subsequent traces at 1-min intervals.

from each other by ~0.19 mm. In this case, the delay between stimulation and excitation increased, and $\dot{V}_{max}$ changed in a biphasic manner, in both cells during octanol treatment. In addition, notches were observed to develop on APs in both cells, and neither cell fired after octanol eventually blocked conduction. Note that the capacitive transients were larger at this distance of microelectrode separation. It is possible that at this interelectrode distance the transient is a combination of stray capacitance (artifact) and capacitive coupling between the cells.

The development of the phase 1 notch during octanol treatment is shown in the series of recordings presented in Fig. 7 *B*. The notch generally developed during the period of $\dot{V}_{max}$ decline, when $\theta$ had dropped below 20 cm/s, and the foot of the AP and input resistance had increased substantially. As $\theta$ declined, the degree of repolarization during the notch increased, frequently reaching a peak value of 25–30 mV.

Decremental propagation was routinely obtained just before block when $\theta$ had fallen below 5–10 cm/s. Abnormal propagation was also occasionally observed. An example, suggestive of reentry, which occurred transiently just before block during octanol treatment is presented in Fig. 8. In this case, an AP originally initiated by the stimulus did not propagate from cell Nos. 1 to 2, however, a subsequent reentrant beat was found to propagate past both recording sites. The pathway for this reentrant excitation was not identified but it was confined within one end of the muscle near the site of stimulation. It also seems likely that the pathway was relatively short given the brief time delay between initial and subsequent beat in cell No. 1.

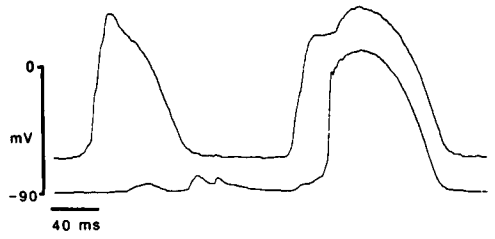


FIGURE 8 Abnormal propagation during octanol treatment. This recording shows an example of abnormal propagation, suggestive of reentry, which occurred just before propagation block at 31 min after the initiation of octanol (0.48 μl/ml) treatment. A single stimulus evoked the AP recorded in cell No. 1 (upper trace; shifted by 20 mV vertically for clarity) which did not propagate to cell No. 2. Before the next stimulus a second beat was recorded in cell No. 1, and in this case it propagated to cell No. 2.

In all cases, reexposure to normal Tyrode solution fully reversed the effects of octanol on $\theta$, $\dot{V}_{max}$, and AP shape (Fig. 6). Only a slight decrease of 2–5 mV in resting membrane potential from a control value of $-89 \pm 0.6$ mV was observed at the concentration of octanol used in these experiments. However, at higher concentrations of octanol (>0.6 μl/ml), the membrane depolarized between 10 and 15 mV before propagation block (not shown).

The decrease in propagation velocity during octanol exposure was associated with a biphasic change in $\dot{V}_{max}$ (Fig. 9). In clear contradiction to the change predicted by continuous cable theory, $\dot{V}_{max}$ first increased to a maximal value, and then subsequently decreased until propagation block occurred. Data for a single experiment are shown in Fig. 6 and the average values of $\dot{V}_{max}$ and $\theta$ for several experiments are shown in Fig. 9. $\dot{V}_{max}$ increased from an average value of 133.1 ± 5.4 in untreated tissues ($\theta$ = 53.2 ± 3.5 cm/s), to a maximal value of 201.7 ± 11.0 V/s when $\theta$ had dropped to 20.5 ± 2.8 cm/s during octanol treatment. As $\theta$ continued to decrease to <6.6 ± 2.1 cm/s

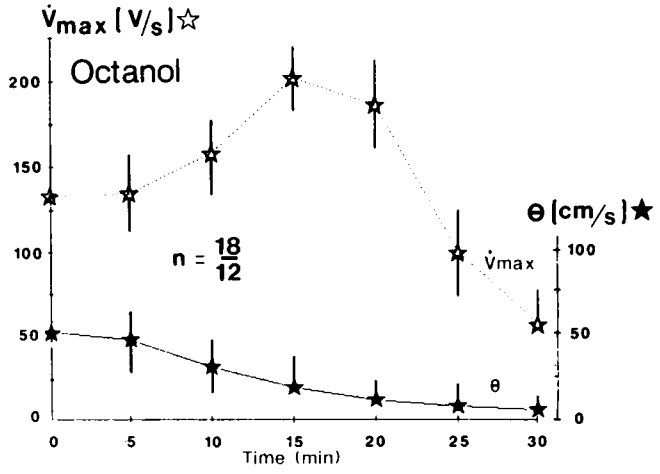


FIGURE 9 Biphasic alteration $\dot{V}_{max}$ during octanol treatment. $\dot{V}_{max}$ (V/s) and $\theta$ (cm/s) are plotted as a function of time in octanol (0.48 μl/ml). Note the biphasic change in $\dot{V}_{max}$ as $\theta$ decreased. Each point is the mean ± SEM ($n$ = 18 cells, 12 tissues).

just before block, $\dot{V}_{max}$ was observed to fall below 100.8 ± 22.1 V/s. In most cases, the peak value for $\dot{V}_{max}$ was achieved just before the initial appearance of prominent notches. A biphasic change in $\dot{V}_{max}$ was also observed during washout and recovery from block in normal Tyrodes solutions.

The input resistance of the impaled cells ($R_{in}$) was found to increase during octanol exposure (Fig. 10 *A*). $R_{in}$ rose from an average value of 4.8 ± 0.8 MΩ in control solution to 49.6 ± 5.6 MΩ when propagation failed. As the input resistance increased and $\theta$ declined, the foot of the AP was found to increase substantially and to become increasingly nonexponential. These changes in the foot are apparent in Figs. 4 and 7. The time constant of the AP foot ($\tau_{foot}$) was calculated to increase from 0.55 ± 0.04 in control solutions to 3.5 ± 0.5 ms ($n$ = 5) in octanol just before propagation block (Fig. 10 *B*). However, it should be noted that these values were calculated on the basis of the slope of the initial 10 mV of depolarization of the foot on semilog plots. In all instances during octanol exposure, this initial slope was not maintained but was followed by a period of even slower voltage change before threshold was reached. For this reason, the values given above should be regarded as the "apparent time constant" of the foot.

The nonexponential rise in voltage during the AP foot was also apparent in phase-plane displays of propagating APs recorded at different times during octanol treatment (Fig. 11). The ascending limb of the phase-plane loop was typically nonlinear in control solutions consisting of at least two phases (Fig. 11). During exposure to octanol this ascending limb always became increasingly nonlinear. This is evident in the loops recorded at 23 and 32 min exposure to octanol in Fig. 11, including a distinct inflection on the ascending limb of the loop at 23 min.

The various effects of octanol on propagation in papillary muscles are attributable to the influence of this agent on gap junctions. Octanol is known to influence other, nonjunctional channels, for example, it enhances Na channel inactivation in nerve (Swenson and Narahashi, 1980; Hirche, 1985). However, this cannot account for the biphasic change in $\dot{V}_{max}$, because the rising phase would have been obscured if significant inactivation had taken place.

## DISCUSSION

Comparison of the results obtained in our simulations and experiments shows that there were parallel changes in propagation velocity ($\theta$), maximal rate of change in upstroke velocity ($\dot{V}_{max}$), AP shape, the foot of the action potential ($\tau_{foot}$), and phase-plane displays under conditions of increased intercellular resistance. This close correlation between theoretical and experimental observations provides strong support for describing longitudinal propagation in cardiac muscle with a discontinuous cable model.

The concept of discontinuous propagation in cardiac tissue arose from studies of the spread of excitation in a

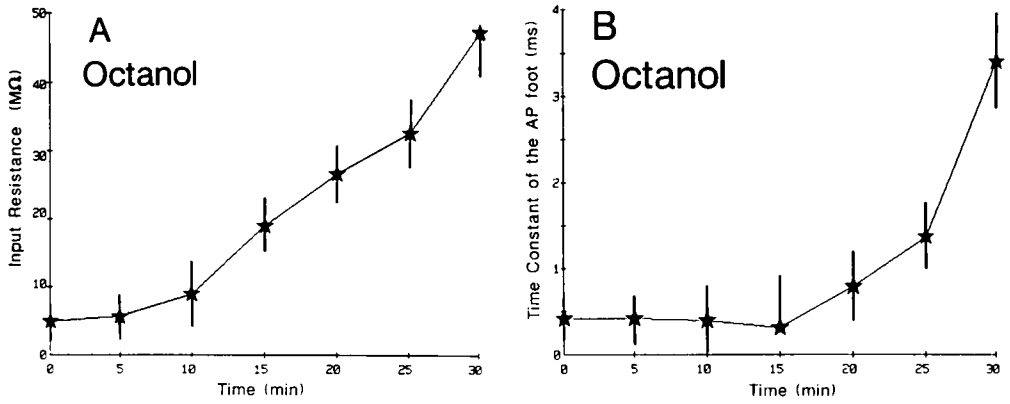


FIGURE 10 Increased input resistance ($R_{in}$) increased time constant of the AP foot during octanol treatment. (*A*) Input resistance ($R_{in}$) (mean ± SEM, $n$ = 12 cells, 6 tissues) plotted as a function of time during octanol (0.48 μl/ml) treatment. (*B*) The time constant of the AP foot is plotted as a function of time during octanol (0.48 μl/ml) treatment. Each point is the mean ± SEM ($n$ = 5 cells, 3 tissues).

transverse direction across atrial tissue (Spach et al., 1981). The inability of continuous cable theory to explain an increase in $\dot{V}_{max}$ associated with depressed conduction velocity led Spach et al. (1981, 1986) to propose that propagation in the transverse direction is discontinuous or "saltatory." That is, the increased effective axial resistance due to sparse lateral gap junctions and infrequent lateral connections between adjacent bundles of muscle fibers produces well-defined hesitations, hence, nonhomogeneous conduction.

In an effort to explain the data of Spach et al. (1981), computer simulations of propagation were conducted using a model based on a one-dimensional strand of cardiac cells in which the discrete nature of the cells was clearly defined (Diaz et al., 1983). $\dot{V}_{max}$ was shown to increase despite slower propagation under conditions of moderately elevated intercellular resistance. These data confirmed a previous observation by Joyner (1982), and were in agreement with the experimental results of Spach et al. (1981). Moreover, they demonstrated that propagation under conditions of high intercellular resistance (i.e., >20 ohm·cm$^2$) was saltatory. That is, it occurred at a high velocity within any given cell, but when viewed over several cells, it proceeded at a considerably slower rate because of a significant time delay at each cell-to-cell boundary. Most of the conduction time is consumed at the gap junctions, even though the cell-to-cell channel is only about one-ten thousandth of the cell length. Excitation appears to jump from one junctional border to the next.

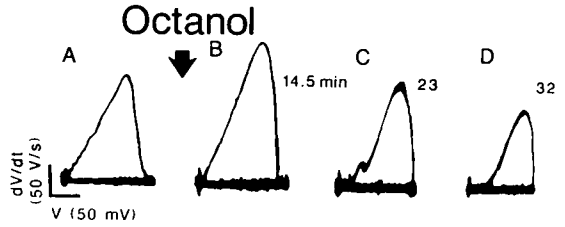


FIGURE 11 Altered phase-plane loops during octanol treatment. Phase-plane loops ($dV/dt$ vs. $V$) for propagating APs are shown for control conditions (*A*) and at 14.5 (*B*), 23 (*C*) and 32 (*D*) min during octanol (0.48 μl/ml) treatment. Note the increasingly nonlinear ascending portion of the loops during exposure to octanol (*B–D*) and distinct inflection on this limb at 23 min (*C*).

The results of our computer simulations are similar to those previously published (Diaz et al., 1983; Rudy and Quan, 1986). These theoretical data predict that the gap junctions have a distinct influence on propagation which is most apparent when the number of channels between adjacent cells is reduced. Our study of the influence of octanol on propagation in papillary muscles provides experimental evidence consistent with these theoretical predictions. Exposure to octanol and decreasing the number of junctional channels slowed propagation and caused a biphasic alteration in $\dot{V}_{max}$ in both the experiments and simulations. These changes were associated with a parallel increase in the foot of the AP, the development of a distinct phase 1 notches, as well as nonlinear and notched ascending limbs on phase-plane displays. These observations, particularly the change in $\dot{V}_{max}$ and phase-plane data, are clearly inconsistent with continuous cable theory. In a continuous cable, alterations in internal resistance should have no effect on $\dot{V}_{max}$ or the linearity of the ascending limb of phase-plane loops.

The biphasic alteration in $\dot{V}_{max}$ with enhanced intercellular resistance can be attributed to changes in the degree of confinement of axial current flow (Joyner, 1982; Rudy and Quan, 1986). When intercellular resistance is increased, axial current flow is suppressed, and more current generated by the active response is forced across the membrane resulting in a greater rate of rise. Eventually, however, $\dot{V}_{max}$ begins to decline when the cells are poorly coupled because of significant Na channel inactivation during the prolonged foot of the AP. This point is supported by our observation that the decline in $\dot{V}_{max}$ is eliminated by slowing the inactivation process.

In this study, propagation in a one-dimensional cable was compared with conduction in small guinea pig papillary muscles. Despite the obvious geometric differences between these two preparations (i.e., a one-dimensional chain and a three-dimensional array of myocytes) the effects on propagation of reducing the number of junctional channels between adjacent cells were found to be qualitatively similar. Some quantitative differences were

noted. For example, $\dot{V}_{max}$ was noted to increase substantially more during uncoupling in the papillary muscle preparations. This may be attributed to the loss of the electrical load of transversely coupled fibers during octanol treatment. The presence of the transversely coupled fibers probably also accounts for the slight differences in propagation velocity at which the peak values of $\dot{V}_{max}$ and conduction block occurred in the simulations and experiments. Temporal and spatial averaging in the papillary muscles may also contribute to these qualitative differences of the wavefront. Future experiments will employ a three-dimensional model in the simulations and will determine axial resistance in both preparations during junctional uncoupling to determine whether qualitatively similar data can be obtained.

The parallel changes in $\tau_{foot}$ observed in our studies are consistent with the simulations of Diaz et al. (1983), but are contrary to the decrease in $\tau_{foot}$ observed experimentally by Spach et al. (1981). However, given the possible structural complexity of the pathway for transverse propagation in cardiac tissue, this is not surprising. Rudy and Quan (1986) suggested that collisions of propagating wavefronts as a result of the complex branching in the transverse direction might lead to a smaller $\tau_{foot}$. Decreased cell length in the transverse direction also produces a smaller $\tau_{foot}$ (Henriquez and Plonsey, 1986; Myers and Maglaveras, 1986).

Notches were observed to develop and lead to a pronounced phase 1 repolarization in propagating APs when intercellular resistance was considerably elevated in both our simulations and experiments. Similar notches were previously observed on APs propagating in a transverse direction across atrial tissue (Spach et al., 1981) and in simulations in which the discrete nature of cardiac cells was considered (Joyner, 1982; Myers and Maglaveras, 1986). They were also observed in frog ventricular tissues bathed in Ca-free Mg Ringer's solution, and were often only present when muscle strips were stimulated at one end but not at the other (Hoshiko and Sperelakis, 1961). This suggests that they are not due to a change in the properties of the excitable membrane. Spach et al. (1981) suggested that because adjacent regions of excitable membrane are only loosely coupled when the intercellular resistance is elevated, the notches could arise from retrograde electrotonic current flow during the firing of the subsequent cell, after the time taken to charge its capacitance. However, this seems unlikely in our case, because slowed Na inactivation in the simulations eliminated the notches. Perhaps they result from significant Na inactivation during the prolonged AP foot, permitting a pronounced repolarization before the Ca current is fully manifest.

Our experiments studying longitudinal propagation in papillary muscles present several observations which are inconsistent with continuous cable theory, but they closely follow the predictions of our simulations which were based on a discontinuous cable model. Thus, the discrete nature of the cells and the influence of the periodic interruptions by the relatively high gap junctional resistances (i.e., compared with myoplasmic resistance) in cardiac tissue must be considered even in an analysis of longitudinal propagation (Freygang and Trautwein, 1970). Under normal conditions, continuous cable theory closely approximates propagation that was observed in the present and previous studies. However, under conditions where coupling begins to be compromised, such as is expected in ischemia, the discontinuous nature of propagation becomes clearly manifest and must be considered to explain conduction data. That continuous cable theory only approximates propagation under normal conditions is evident from its inability to account for the nonlinear ascending portion of phase-plane loops recorded from many cardiac cells, including cells in the Purkinje system (Fig. 11 in present study; Sperelakis and Shumaker, 1968; Paes de Carvalho et al., 1969; Paes de Carvalho, 1975; Paes de Carvalho et al., 1982). Slight nonlinear ascending limbs were observed in our simulations and experiments under control conditions, and these became more apparent, and notched, as junctional resistance was increased and propagation slowed (Fig. 11). The delay in propagation at the cleft under normal conditions is short, as shown in Fig. 2 *A*. However, this delay or hesitation likely accounts for the slight nonlinearity in the ascending limb. Significantly, the inflections which we observed under uncoupled conditions are similar to those obtained from cells in the AV node (Paes de Carvalho et al., 1969) where propagation velocity was similarly $<10$ cm/s. It is clear that conduction in cardiac muscle is not homogeneous even under control conditions, and that increasing junctional resistance only enhances this nonhomogeneity.

In summary, this study provides evidence supporting the concept of discontinuous propagation in the heart. Depressed propagation due to decreased numbers of gap junction channels between adjacent cells is associated with biphasic alterations in $\dot{V}_{max}$ and increasingly nonlinear ascending limbs of phase-plane loops. These data cannot be explained on the basis of classical continuous cable theory. Thus, in our attempts to model and analyze propagation in cardiac muscle under normal and pathological conditions such as ischemia, the discontinuous nature of conduction in this tissue should be considered.

The authors thank Ms. Rhonda Hentz and Ms. Anita Tolle for their labors in the preparation of this manuscript and Mr. P. Goosmann for the artwork.

Dr. W. C. Cole thanks the Canadian Heart Foundation for support in the form of a Junior Fellowship. J. Picone is a predoctoral trainee supported by grant HL-07571 from National Institutes of Health. We thank the CLINFO Computer Center at the University of Cincinnati College of Medicine for the generous use of their computer facilities. This study was supported by National Institues of Health grant HL-31942.

*Received for publication 2 July 1987 and in final form 29 December 1987.*

## REFERENCES


Beeler, G. W., and H. Reuter. 1977. Reconstruction of the action potential of ventricular myocardial fibers. *J. Physiol. (Lond.).* 268:177–210.

Bernardini, G., C. Peracchia, and L. L. Peracchia. 1984. Reversible effects of heptanol on gap junction structure and cell-to-cell electrical coupling. *Eur. J. Cell Biol.* 34:307–312.

Bonke, F. I. M. 1973. Passive electrical properties of atrial fibers of the rabbit heart. *Pfluegers Arch. Eur. J. Physiol.* 339:1–15.

Carmeleit, E., and J. Willems. 1971. The frequency dependent character of the membrane capacity in cardiac Purkinje fibers. *J. Physiol. (Lond.).* 213:85–93.

Clerc, L. 1976. Directional difference of impulse spread in trabecular muscle from mammalian heart. *J. Physiol. (Lond.).* 255:335–346.

Cole, W. C., J. B. Picone, and N. Sperelakis. 1987. Gap junctional uncoupling and discontinuous propagation in the heart: a comparison of experimental data with computer simulations. American Heart Annual Meeting, Anaheim, CA. (Abstr.)

Crank, J., and P. Nicholson. 1947. A practical method for numerical evaluation of solutions of partial differential equations of the heat conduction type. *Proc. Cambridge Philos. Soc. (Math. Phys. Sci.).* 43:50–67.

Déleže, J., and J. C. Hervé. 1986. Quantitative gap junction alterations in mammalian heart cells quickly frozen or chemically fixed after electrical coupling. *J. Membr. Biol.* 93:11–21.

DeMello, W. C. 1977. Passive electrical properties of the atrioventricular node. *Pfluegers Arch. Eur. J. Physiol.* 371:135–139.

Diaz, P. J., Y. Rudy, and R. Plonsey. 1983. Intercalated discs as a cause for discontinuous propagation in cardiac muscle: a theoretical simulation. *Ann. Biomed. Eng.* 11:177–189.

Freygang, W. H., and W. Trautwein. 1970. The structural implications of the linear electrical properties of cardiac Purkinje strands. *J. Gen. Physiol.* 55:524–547.

Forbes, M. S., and N. Sperelakis. 1985. Intercalated discs of mammalian heart: a review of structure and function. *Tissue & Cell.* 17:605–648.

Henriquez, C. S., and R. Plonsey. 1986. The effect of junctional discontinuities on cardiac propagation. *IEEE (Inst. Electr. Electron. Eng.) Eighth Annu. Conf. Eng. Med. Biol. Soc. Proc.* 244–246.

Heppner, D. B., and R. Plonsey. 1970. Simulation of electrical interaction of cardiac cells. *Biophys. J.* 10:1057–1075.

Hirche, G. 1985. Blocking and modifying actions of octanol on Na channels in frog myelinated nerve. *Pfluegers Arch. Eur. J. Physiol.* 405:180–187.

Hodgkin, A. L., and W. A. H. Rushton. 1946. The electrical constants of a crustacean nerve fiber. *Proc. R. Soc. Lond. B Biol. Sci.* 133:444–479.

Hodgkin, A. L., and A. F. Huxley. 1952. A quantitative description of membrane current and its application to conduction and excitation in nerve. *J Physiol. (Lond.).* 117:500–544.

Hoshiko, T., and N. Sperelakis. 1961. Prepotentials and unidirectional propagation in myocardium. *Am. J. Physiol.* 201:873–880.

Johnston, M. F., S. A. Simon, and F. Ramon. 1980. Interaction of anaesthetics with electrical synapses. *J. Physiol. (Lond.).* 286:498–500.

Joyner, R. W. 1982. Effects of discrete electrical coupling on propagation through an electrical syncytium. *Circ. Res.* 50:192–200.

Joyner, R. W., and E. D. Overholt. 1985. Effects of octanol on canine subendocardial Purkinje-ventricular transmission. *Am. J. Physiol.* 249:H1228–H1231.

Joyner, R. W., R. M. Westerfield, J. W. Moore, and N. Stockbridge. 1978. A numerical method to model excitable cells. *Biophys. J.* 22:155–170.

Katz, B. 1966. Nerve, Muscle, and Synapse. McGraw-Hill Book Co., New York.

Mann, J. E., E. Foley, and N. Sperelakis. 1977. Resistance and potential profiles in the cleft between two myocardial cells. Electrical analog and computer simulations. *J. Theor. Biol.* 68:1–15.

Myers, G. A., and M. Maglaveras. 1986. Cardiac action potential propagation is discontinuous. *IEEE (Inst. Electr. Electron. Eng.) Eighth Annu. Conf. Eng. Med. Biol. Soc. Proc.* 241–243.

Paes de Carvalho, A. 1975. Phase-plane determination of membrane currents in propagated action potentials: possibilities and difficulties. *In* Concepts of Membranes in Regulation and Excitation. M. Rochae Silva and G. Suarez-Kurtz, editors. Raven Press, New York. 85–96.

Paes de Carvalho, A., B. F. Hoffman, and M. Paula Carvalho. 1969. Two components of the cardiac action potential. I. Voltage time course and the effect of acetylcholine on atrial and nodal cells of the rabbit heart. *J. Gen. Physiol.* 54:607–635.

Paes de Carvalho, A., T. A. Saldena, E. A. C. Garcia, A. C. Campos de Carvalho, T. Tashiro, and M. de Paulo Carvalho. 1982. Homogeneous and nonhomogeneous conduction of impulses in heart and other tissues. *In* Normal and Abnormal Conduction in the Heart. A. Paes de Carvalho, B. F. Hoffman, and M. Lieberman, editors. Futura Publishing Co., New York. 117–144.

Picone, J., W. Cole, and N. Sperelakis. 1987. Effects of altered gap junctional coupling on propagation in a discontinuous cable model of cardiac muscle: a comparison of computer simulations with experimental data. FASEB (Fed. Am. Soc. Exp. Biol.) Meeting. Washington, DC. (Abstr.)

Rudy, Y., and W.-L. Quan. 1987. Effects of the discrete cellular structure on electrical propagation in cardiac tissue. *In* Electromechanical Activation, Metabolism, and Perfusion of the Heart-Simulation and Experimental Models. S. Sideman and R. Beyar, editors.

Sharp, G., and R. W. Joyner. 1980. Numerical simulations of propagating cardiac action potentials. *Biophys. J.* 31:403–424.

Spach, M. S., W. T. Miller, D. B. Geselowitz, R. C. Barr, J. M. Kootsey, and E. A. Johnson. 1981. The discontinuous nature of propagation in normal canine cardiac muscle. *Circ. Res.* 48:39–54.

Spach, M. S., and P. C. Dolber. 1986. Relating extracellular potentials and their derivatives to anisotropic propagation at a microscopic level in human cardiac muscle. Evidence for electrical uncoupling of side-to-side fiber connections with increasing age. *Circ. Res.* 58:356–371.

Sperelakis, N., and H. K. Shumaker. 1968. Phase-plane analysis of cardiac action potentials. *J. Electrocardiol.* 1:31–42.

Swenson, R. P., and T. Narahashi. 1980. Block of Na conductance by *n*-octanol in crayfish giant axon. *Biochim. Biophys. Acta.* 603:228–236.

Veenstra, R. D., and R. L. DeHaan. 1986. Measurement of single channel currents from cardiac gap junctions. *Science (Wash. DC).* 233:972–974.

Weidmann, S. 1952. The electrical constants of Purkinje fibers. *J. Physiol. (Lond.).* 118:348–360.

Weidmann, S. 1970. Electrical constants of trabecular muscle from mammalian heart. *J. Physiol. (Lond.).* 210:1041–1054.

Woodbury, J. W., and W. E. Crill. 1961. On the problem of impulse conduction in theatrium. *In* Nervous Inhibition. E. Florey, editor. Pergamon Press, Oxford. 124–135.

White, R. L., D. C. Spray, A. C. Campos de Carvalho, B. A. Wittenberg, and M. V. L. Bennett. 1985. Some electrical and pharmacological properties of gap junctions between adult ventricular myocytes. *Am. J. Physiol.* 249:C447–C455.